Spontaneous Velocity Alignment in Motility-Induced Phase Separation

L. Caprini,[1] U. Marini Bettolo Marconi,[2] and A. Puglisi[3]
[1]Gran Sasso Science Institute (GSSI), Via. F. Crispi 7, 67100 L'Aquila, Italy
[2]Scuola di Scienze e Tecnologie, Università di Camerino—via Madonna delle Carceri, 62032 Camerino, Italy
[3]Istituto dei Sistemi Complessi—CNR and Dipartimento di Fisica, Università di Roma Sapienza, P.le Aldo Moro 2, 00185 Rome, Italy

(Received 3 October 2019; revised manuscript received 6 December 2019; accepted 29 January 2020; published 19 February 2020)

We study a system of purely repulsive spherical self-propelled particles in the minimal setup inducing motility-induced phase separation (MIPS). We show that, even if explicit alignment interactions are absent, a growing order in the velocities of the clustered particles accompanies MIPS. Particles arrange into aligned or vortexlike domains whose size increases as the persistence of the self-propulsion grows, an effect that is quantified studying the spatial correlation function of the velocities. We explain the velocity alignment by unveiling a hidden alignment interaction of the Vicsek-like form, induced by the interplay between steric interactions and self-propulsion.

DOI: 10.1103/PhysRevLett.124.078001

Fishes [1], birds [2], or insects [3] often display fascinating collective behaviors such as flocking [2,4] and swarming [5], where all units of a group move coherently, producing intriguing dynamical patterns. A different mode of organization of living organisms is clustering, for instance in bacterial colonies [6], such as *E. coli* [7], *Myxococcus xanthus* [8], or *Thiovulum majus* [9], relevant for histological cultures in several areas of medical and pharmaceutical sciences. Out of the biological realm, the occurrence of stable clusters [10–13], stable chains [14], or vortices [15] in activated colloidal particles, e.g., autophoretic colloids or Janus disks [16,17], offers an interesting challenge for the design of new materials.

Even if the microscopic details differ case by case, a few classes of minimal models with common coarse-grained features have been introduced in statistical physics. Units in these models are called "active" or "self-propelled" particles [18–20] to differentiate them from Brownian colloids which passively obey the forces of the surrounding environment. Propelling forces may be either of mechanical origin (flagella or body deformation), or thermodynamic nature (diffusiophoresis and self-electrophoresis) [21,22]. In some simple and effective examples, self-propulsion is modeled as a constant force with stochastic orientation, as in the case of active Brownian particles (ABP) [23,24]. Thermal fluctuations play only a marginal role and stochasticity is usually due to the unsteady nature of the swimming force itself.

The recent theoretical activity has focused on two kinds of ordering phenomena in active matter: (i) density phase-separation and (ii) orientation (or velocity) alignment. We review some essential points of the two phenomena, useful in the Letter. Concerning case (i), the interplay between steric interactions and self-propulsion is believed to be sufficient for observing phase separation as density or activity increases. This occurs even in the absence of attractive forces, at variance with passive Brownian particles, and for this reason the mechanism is known as motility-induced phase separation (MIPS) [25,26]. Originally rationalized in the framework of run and tumble models, it has been recently recognized to appear also in ABP [27,28]. Regarding case (ii), the appearance of any kind of order in the orientation or velocity of active particles is deemed to be a consequence of some breaking of microscopic isotropy or the introduction of explicit aligning interactions. For instance it may occur for dumbbells, rods, and, in general, elongated microswimmers even in the absence of explicit alignment interactions [29–32]. Explicit interactions that favor the alignment of neighbors' velocities of course induce the emergence of ordering in the velocity field also for spherical particles, such as in the seminal Vicsek model [33,34], where a transition to long-range order ("flocking") has been put in evidence [35–37], together with density inhomogeneities in the form of traveling bands [38,39] or periodic density waves [40]. In recent years, a new ordering mechanism has been recognized, which has been termed implicit or self-alignment: the orientation of the particle tends to align to its velocity, and this (without additional explicit aligning particle-particle interactions) produces orientation-velocity ordering [41,42].

Summarizing, the alignment characterizing Vicsek-like models and the MIPS-like phase separation are phenomena that are usually thought to be distinct. The effect of velocity-velocity aligning interactions for the MIPS scenario has been also considered, but a clear effect of their interplay is still an open question [43–47].

In the present Letter, we challenge the widespread idea that explicit alignment interactions are necessary to observe a growing orientational order or—equivalently—that the

velocity alignment observed in Vicsek-like models do not appear in purely repulsive, spherical ABP particles. To the best of our knowledge, previous studies aimed to measure the polarization, i.e., the existence of a common orientation of the self-propelling force, but they overlooked the possibility of ordering in the real particles' velocity, which is the crucial observation of the present Letter.

We consider a system of N interacting self-propelled particles, for simplicity (and without loss of generality) in two dimensions. The evolution of the center of mass coordinate of each of them, $\mathbf{x}_i$, is described by an overdamped equation of motion with self-propulsion embodied by a time-dependent external force with constant modulus, v_0, and orientation vector, $\mathbf{n}_i$, of components $(\cos\theta_i, \sin\theta_i)$. According to the ABP scheme, the orientational angles, θ_i, evolve as independent Wiener processes. Interactions are purely repulsive and no explicit aligning forces are included. Therefore, the dynamics reads:

$$\gamma\dot{\mathbf{x}}_i = \mathbf{F}_i + \gamma v_0 \mathbf{n}_i, \tag{1a}$$

$$\dot{\theta}_i = \sqrt{2D_r}\xi_i, \tag{1b}$$

D_r being the rotational diffusivity (thermal diffusion is usually negligible) while γ is the constant drag coefficient. Steric interactions are modeled by the force $\mathbf{F}_i = -\nabla_i U_{\mathrm{tot}}$, being $U_{\mathrm{tot}} = \sum_{i<j} U(|\mathbf{r}_{ij}|)$ with $\mathbf{r}_{ij} = \mathbf{x}_i - \mathbf{x}_j$. We choose $U(r)$ as a purely repulsive potential of the WCA type, namely $U(r) = 4\epsilon[(\sigma/r)^{12} - (\sigma/r)^6] + \epsilon$, for $r \leq 2^{1/6}\sigma$ and zero otherwise. The constant σ represents the nominal particle diameter while ϵ is the energy scale of the interactions.

Numerical integration of Eq. (1a) is performed for a system of N particles in a square box of length L (which does not exceed the persistence length v_0/D_r except for $1/D_r = 3,\ 5$), with periodic boundary conditions. We consider a packing fraction $\phi = 0.64$, where MIPS is known to occur at small enough values of D_r [27]. Indeed, Fig. 1(a) shows the coexistence of a stable dense cluster and a dilute disordered phase, at $D_r = 0.2$. The boundary of the cluster is highly dynamical: continuously in time, particles join or leave the cluster, in such a way that its average population remains stable. In Figs. 1(b)–1(d), we enlarge three representative regions of the system. The bulk displays a highly ordered close-packing configuration [28]. The pair correlation function, $g(r)$, shown in the Supplemental Material [48], reveals that within the cluster the main peak occurs at a distance $\bar{r} < \sigma$: particles attain a steady-state configuration with large potential energy, where each self-propelled particle climbs on the repulsive potential exerted by the surrounding ones. Besides, the occurrence of a second double-split peak reveals a hexagonal lattice structure, in agreement with the direct observation and previous studies [28]. The colors in Figs. 1(a)–1(d) encode the orientation, $\mathbf{n}$,

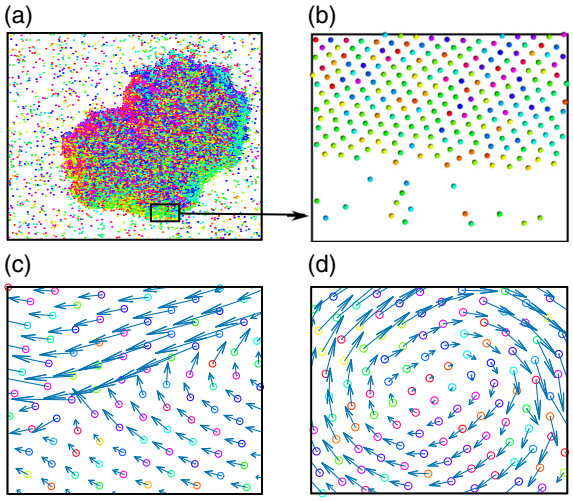

FIG. 1. In panel (a) we plot a snapshot configuration, displaying MIPS, enlarging a window near the surface of the cluster in panel (b). Colors encode the self-propulsion direction. Panels (c) and (d) are windows of the bulk where we plot the velocities of each particle with blue arrows, showing aligned and vortex domains, respectively. Data are obtained by simulation with $v_0 = 50$, $D_r = 0.2$ and the other parameters as described in the text.

of the self-propelling force which appears to lack any kind of alignment.

In Figs. 1(c) and 1(d) we give evidence of the main novel phenomenon reported here. We draw with blue arrows the velocities, $\dot{\mathbf{x}}_i$, of each active particle which in general is different from the orientation of the active force, i.e., $\dot{\mathbf{x}}_i \neq \mathbf{n}_i v_0$. Despite the absence of any alignment interaction, the velocities of the self-propelled particles in the bulk of the cluster align, self-organizing in large oriented domains inside the cluster. Even if each $\mathbf{n}_i$ points randomly, particles in large groups move in the same direction [Fig. 1(c)]. Such domains dynamically self-arrange continuously in time and, in some cases, evolve into vortex structures as evidenced in Fig. 1(d). The average velocity of each domain is quite smaller than v_0 (the typical speed in the absence of interactions). Further details about the velocity distributions in the different phases are contained in the Supplemental Material [48].

The global alignment of the particles or polarization is commonly measured by considering the propulsion orientation, $\mathbf{n}_i$, of each particle, while here we focus on the velocity $\dot{\mathbf{x}}_i$. A possible order parameter is represented by the sum $|\sum_{k=1}^{N} e^{i\psi_k(t)}|/N$, where ψ_k is the angle formed by the particle velocity with respect to the x axis. Such a parameter has the property of being zero for particles without any alignment while it returns one for perfectly aligned particles. Unfortunately, even if restricted to particles inside a cluster, such a quantity does not reveal a clear polarization of the system because of the presence of several domains with different orientations. Thus, we introduce the spatial correlation function of the velocity

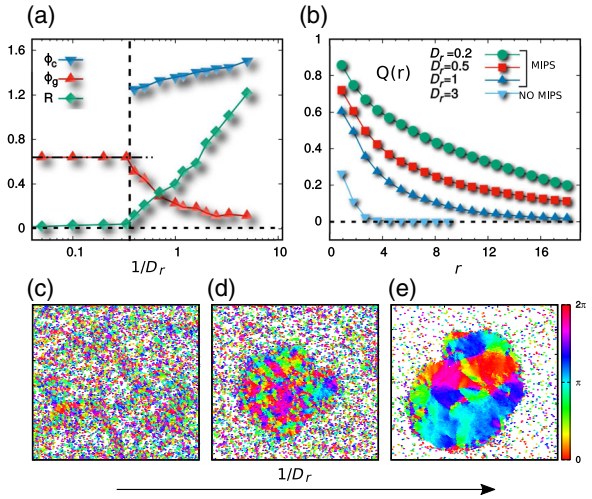

FIG. 2. Panel (a): density, ϕ_g (red upper triangles) and ϕ_c (blue lower triangles) for the dilute and the cluster phase, respectively, as a function of $1/D_r$. Velocity-alignment order parameter, R (green diamonds), as a function of $1/D_r$. For presentation reasons, R is rescaled by a factor 6. Black dashed lines are eye-guides: the vertical one identifies the value of $1/D_r$ at which the MIPS-transition occurs. Instead, the horizontal lines refer to the nominal density (∼0.64) and the value of R in absence of velocity alignment (∼0). Panel (b): $Q(r)$ for different values of D_r, as shown in the legend, where we specify the presence or not of the phase separation. Panels (c), (d), and (e): snapshot configurations for three different values of $1/D_r$. Panel (c) is obtained for $D_r = 3$, panel (d) for $D_r = 1$, and panel (e) for $D_r = 0.2$. Colors are associated with the direction of the velocity of each particle. All the simulations are realized with numerical density ∼0.64, $v_0 = 50$ and the other parameters specified in the text.

orientation, $Q_i(r)$. We define the angular distance between two angles $d_{ij} = \min[|\psi_i - \psi_j|, 2\pi - |\psi_i - \psi_j|]$, and measure the velocity alignment between particle i and the neighboring particles in the circular crown of mean radius $r = k\bar{r}$, with integer $k > 0$, and thickness $\bar{r}$, in such a way that

$$Q_i(r) = 1 - 2\sum_j \frac{d_{ij}}{\mathcal{N}_k \pi}, \tag{2}$$

where the sum runs only over the particles in the circular shell selected by k and $\mathcal{N}_k$ is the number of particles in it. Then, we define $Q(r) = \sum_i Q_i(r)/N$, which reads 1 for perfectly aligned particles in the kth shell, -1 for anti-aligned particles, and 0 in the absence of any form of alignment. $Q(r)$ quantifies partial alignment even in the absence of global polarization. Panel (b) of Fig. 2 shows $Q(r)$ for different values of D_r in a set of simulations with $v_0 = 50$ (the remaining parameters are fixed as above). In general, Q is a decreasing function of r. At large D_r where MIPS does not occur, the alignment measured by $Q(r)$ is absent or very weak, affecting no more than the first two shells. In the MIPS configuration, the degree of alignment increases and spans larger and larger distances, when D_r is reduced. Three snapshots with color-encoded velocity orientation are shown in Figs. 2(c)–2(e), showing the growth of velocity-aligned domains in the cluster phase. In Fig. 2(a) we investigate the nature of this ordering phenomenon by measuring the following order parameter

$$R = \int Q(r) dr. \tag{3}$$

The integral is performed over the whole cluster domain while in the absence of phase separation we consider the whole box.

To evaluate the relationship between this growing spatial velocity order and MIPS, we compare R with an established order parameter for phase separation. Local packing fractions show a unimodal distribution when the system is not phase separated and a bimodal one when phase separation occurs. The height of the peaks in the distribution identifies the most probable values of the packing fraction in the unimodal case, it corresponds to the homogeneous phase $\phi_g \approx \phi$. Instead, in the bimodal case, the cluster phase is identified by the peak with $\phi_c > \phi$ while the disordered phase by that with $\phi_g < \phi$. These results are reproduced as a function of $1/D_r$ in Fig. 2(a). At $1/D_r \sim 0.3$ phase separation is revealed by the transition from a single peak to a double peak in the distribution of the packing fraction. In our configuration, ϕ_g in the homogeneous phase follows continuously the values outside the cluster, which forms at a much higher packing fraction. The comparison with the curve for R reveals the most interesting information of our study, which is the coincidence between the MIPS transition and the growing of the velocity order. Indeed, R reveals a two-steps behavior, being almost zero before $1/D_r \sim 0.3$ and revealing a sharp, monotonic increase starting from this point. The reason for such an increase is twofold: a pure nonequilibrium effect induced by the growing of $1/D_r$ (relevant even at constant density) and the slow increase of ϕ_c, shown in Fig. 2(a). Such a distinction is confirmed in the Supplemental Material [48], where we study an active system with periodic boundary conditions at a higher density where no phase separation is present. Even in this case, domains with velocity alignment are observed, whose size increases with $1/D_r$.

To shed light on the above phenomenology we perform an exact mapping of the original ABP dynamics, Eq. (1), in the same spirit of the Ornstein-Uhlenbeck (AOUP) model [49–51]. In particular, we obtain an equation of motion for the active particle velocity, $\mathbf{v}_i = \dot{\mathbf{x}}_i$, which is an unprecedented result for ABP. In two dimensions, $\mathbf{v}_i$ follows:

$$\mu\dot{\mathbf{v}}_i = -\gamma \sum_{j=1}^{N} \Gamma_{ij}(\mathbf{r}_{ij})\mathbf{v}_j + \mathbf{F}_i + \sqrt{2\gamma(\mu v_0^2)}\boldsymbol{\xi}_i \times \mathbf{n}_i, \tag{4}$$

where $\boldsymbol{\xi}_i$ is the stochastic vector with components $(0, 0, \xi_i)$ and both $\mathbf{v}_i$ and $\mathbf{x}_i$ belong to the plane xy. The effective mass is $\mu = \gamma/D_r$ and the viscosity matrix Γ_{ij} has the following structure:

$$\Gamma_{ij}^{\alpha\beta}(\mathbf{r}_{ij}) = \delta_{ij}\delta_{\alpha\beta} + \frac{1}{D_r\gamma}\nabla_{i\alpha}\nabla_{j\beta}\sum_{k<l}U(|\mathbf{r}_{kl}|), \quad (5)$$

where Latin and Greek indices refer to the particle number and the spatial vector components, respectively. The derivation of Eq. (4) is reported in the Supplemental Material [48]. Equation (4) is the equation of motion of an underdamped particle under the action of a space-dependent Stokes force and a multiplicative noise both in the velocity and in the position of the target particle. The noise term always acts perpendicularly to $\mathbf{n}_i$. The most interesting information contained in Eq. (4) is the fact that the dynamics of the ith particle is strongly influenced not only by the positions but also by the velocities of the surrounding particles, through the matrix Γ_{ij} which—because of the factor $1/D_r$—is dominated by the velocity coupling terms. We recall that Eq. (4) is almost identical to the equation of motion of interacting AOUP particles [52], the only difference being the noise term, which in the AOUP model is additive and uncorrelated; i.e., $\boldsymbol{\xi}_i \times \mathbf{n}_i$ is replaced by a noise vector with independent components.

Inside a cluster Eq. (4) can be further simplified, taking advantage of the hexagonal spatial order: we may assume that the ith particle in the bulk of the cluster has six neighbors at relative positions $\bar{\mathbf{r}}_{ij}$ with $j = 1, \ldots, 6$, and common distance $\bar{r} = |\bar{\mathbf{r}}_{ij}| < \sigma$, as revealed, for instance, by the $g(r)$. With such an assumption, one gets for the particle at the center of the hexagon

$$\mu\dot{\mathbf{v}} = -\frac{1}{D_r}\sum_{j=1}^{6}\hat{H}_j(\mathbf{v}-\mathbf{v}_j) - \gamma\mathbf{v} + \sqrt{2\gamma(\mu v_0^2)}\boldsymbol{\xi}\times\mathbf{n}, \quad (6)$$

where $\hat{H}_j$ is the matrix coupling the central particle to the jth particle and its elements depend on $\bar{r}$ and on the angle formed by $\mathbf{x}_{ij} = \mathbf{x}_j - \mathbf{x}_i$ and the x axis, as reported in the Supplemental Material [48]. Equation (6) can be rewritten in terms of the average velocity vector of the six neighbors $\mathbf{v}^* = \sum_{j=1}^{6}\mathbf{v}_j/6$ and takes the form

$$\mu\dot{\mathbf{v}} = -\frac{\hat{J}}{D_r}(\mathbf{v}-\mathbf{v}^*) + \frac{1}{D_r}\sum_{j=1}^{6}\hat{H}_j(\mathbf{v}_j-\mathbf{v}^*) - \gamma\mathbf{v} + \mathbf{k}, \quad (7)$$

with $\hat{J} = \sum_j^6 \hat{H}_j = 3\{U''(\bar{r}) + [U'(\bar{r})/|\bar{r}|]\}\mathcal{I}$, being $\mathcal{I}$ the identity matrix and $\mathbf{k}$ the noise vector of Eq. (6). Equations (6) and (7) are derived in the Supplemental Material [48]. We notice that $(U''(\bar{r}) + [U'(\bar{r})/|\bar{r}|]) > 0$ which means that the first term in the rhs of Eq. (7) is a Vicsek-like force aligning the velocity of the central particle towards the average velocity vector $\mathbf{v}^*$ [38]. In two special cases, the second force in the rhs of Eq. (7) vanishes (i) trivially when the six neighbors have identical velocities $\mathbf{v}_j = \mathbf{v}^*$, and (ii) when the six neighbors have velocities arranged according to a vortexlike pattern. This statement is proved in the Supplemental Material [48]. In both cases, at large $1/D_r$ the dynamics of $\mu\dot{\mathbf{v}}$ is dominated by the Vicsek-like aligning force [first term in the rhs of Eq. (7)] and one has a rapid convergence $\mathbf{v} \to \mathbf{v}^*$. At the end of such process—i.e., when the velocity of the central particle is exactly aligned with the six neighbors—the aligning force disappears and the subdominant bathlike terms $-\gamma\mathbf{v} + \sqrt{2\gamma(\mu v_0^2)}\boldsymbol{\xi}\times\mathbf{n}$ perturb the velocity. At this stage, the Vicsek-like force comes back into play and restores the alignment. For more general cases (i.e., when the six neighbors are not aligned or are arranged in a vortex pattern), a second force, depending on the deviations $\mathbf{v}_j - \mathbf{v}^*$ with a large prefactor $1/D_r$, comes into play. However, when particles are close to alignment, the terms $\mathbf{v}_j - \mathbf{v}^*$ are small and uncorrelated, so that their sum is even smaller and does not alter significantly the aligning term, as numerically checked. A rigorous general estimate of the fate of Eq. (7) is difficult. We also note that our analytical description in terms of velocity dynamics could be adapted to describe the emergent polar order of rodlike [31,53,54] or dumbbell [55,56] particles.

To derive the exponential-like form of the spatial velocities correlations, we assume all particles sitting on an infinite hexagonal lattice, with each particle's velocity connected to its six neighbors by Eq. (6). Since $\mathbf{n}$ and $\mathbf{v}$ are roughly uncorrelated in the bulk, we replace the multiplicative noise with an additive uncorrelated noise, as in the AOUP case [57]. The evolution of this velocity field can be mapped, by Fourier transforming, onto a Langevin equation for each mode in the reciprocal lattice. Its steady-state solution gives the velocity structure factor or, equivalently, the spatial correlations of the velocity field. This analysis demonstrates that the correlation length of the velocity field reads

$$\lambda_s \approx \bar{r}\left[\frac{3}{4\gamma D_r}\left(U''(\bar{r}) + \frac{U'(\bar{r})}{|\bar{r}|}\right)\right]^{1/2}, \quad (8)$$

whose derivation is reported in the Supplemental Material [48]. This argument suggests a correlation length growing with $1/D_r$ in qualitative agreement with Figs. 2(a) and 2(b) increasing also as ϕ_c grows through $\bar{r}$. We suspect that terms at small wavelengths can be important, for instance, in the explanation of the vortex structures.

Our study demonstrates an unprecedented strong connection between velocity ordering and MIPS transitions. In the absence of any microscopic force that explicitly aligns velocities, we observe the emergence of velocity patterns, aligned or vortex-like domains in a dense cluster, which become more and more pronounced as the persistence of the active force increases. We stress here the deep nonequilibrium nature of the system. Such a velocity order cannot be observed in any passive Brownian suspensions of spherical particles, since, in those cases, particles' velocities are distributed according to independent Boltzmann

distributions. Thus, the growth of order in the velocity field cannot be explained in equilibriumlike theories unless an effective aligning force is introduced in a macroscopic "Hamiltonian," which is absent in the microscopic model, in analogy with previous equilibriumlike approaches where effective attractive interactions were introduced to explain phase separation [58,59], which are also at the level of an effective free-energy functional [60–63] or employing an effective Cahn-Hilliard equation [64,65]. Such equilibriumlike strategies were challenged by observations about pressure [66,67], negative interfacial tension between the coexisting phases [68,69], and different temperatures inside and outside the cluster [70]. The phenomenology revealed here represents, in our opinion, an additional argument in favor of a purely nonequilibrium approach.

[1] A. J. Ward, D. J. Sumpter, I. D. Couzin, P. J. Hart, and J. Krause, Proc. Natl. Acad. Sci. U.S.A. **105**, 6948 (2008).

[2] M. Ballerini, N. Cabibbo, R. Candelier, A. Cavagna, E. Cisbani, I. Giardina, V. Lecomte, A. Orlandi, G. Parisi, A. Procaccini *et al.*, Proc. Natl. Acad. Sci. U.S.A. **105**, 1232 (2008).

[3] A. Attanasi, A. Cavagna, L. Del Castello, I. Giardina, S. Melillo, L. Parisi, O. Pohl, B. Rossaro, E. Shen, E. Silvestri *et al.*, Phys. Rev. Lett. **113**, 238102 (2014).

[4] T. Mora, A. M. Walczak, L. Del Castello, F. Ginelli, S. Melillo, L. Parisi, M. Viale, A. Cavagna, and I. Giardina, Nat. Phys. **12**, 1153 (2016).

[5] A. Cavagna, D. Conti, C. Creato, L. Del Castello, I. Giardina, T. S. Grigera, S. Melillo, L. Parisi, and M. Viale, Nat. Phys. **13**, 914 (2017).

[6] D. Dell'Arciprete, M. Blow, A. Brown, F. Farrell, J. S. Lintuvuori, A. McVey, D. Marenduzzo, and W. C. Poon, Nat. Commun. **9**, 4190 (2018).

[7] H. Berg, *E. Coli in Motion* (Springer Science & Business Media, 2008).

[8] F. Peruani, J. Starruß, V. Jakovljevic, L. Søgaard-Andersen, A. Deutsch, and M. Bär, Phys. Rev. Lett. **108**, 098102 (2012).

[9] A. P. Petroff, X.-L. Wu, and A. Libchaber, Phys. Rev. Lett. **114**, 158102 (2015).

[10] J. Bialké, T. Speck, and H. Löwen, J. Non-Cryst. Solids **407**, 367 (2015).

[11] J. Palacci, S. Sacanna, A. Steinberg, D. Pine, and P. Chaikin, Science, **339**, 936 (2013).

[12] I. Buttinoni, J. Bialké, F. Kümmel, H. Löwen, C. Bechinger, and T. Speck, Phys. Rev. Lett. **110**, 238301 (2013).

[13] F. Ginot, I. Theurkauff, F. Detcheverry, C. Ybert, and C. Cottin-Bizonne, Nat. Commun. **9**, 696 (2018).

[14] J. Yan, M. Han, J. Zhang, C. Xu, E. Luijten, and S. Granick, Nat. Mater. **15**, 1095 (2016).

[15] A. Bricard, J.-B. Caussin, D. Das, C. Savoie, V. Chikkadi, K. Shitara, O. Chepizhko, F. Peruani, D. Saintillan, and D. Bartolo, Nat. Commun. **6**, 7470 (2015).

[16] J. R. Howse, R. A. L. Jones, A. J. Ryan, T. Gough, R. Vafabakhsh, and R. Golestanian, Phys. Rev. Lett. **99**, 048102 (2007).

[17] S. C. Takatori, R. De Dier, J. Vermant, and J. F. Brady, Nat. Commun. **7**, 10694 (2016).

[18] M. C. Marchetti, J. F. Joanny, S. Ramaswamy, T. B. Liverpool, J. Prost, M. Rao, and R. A. Simha, Rev. Mod. Phys. **85**, 1143 (2013).

[19] S. Ramaswamy, Annu. Rev. Condens. Matter Phys. **1**, 323 (2010).

[20] C. Bechinger, R. Di Leonardo, H. Löwen, C. Reichhardt, G. Volpe, and G. Volpe, Rev. Mod. Phys. **88**, 045006 (2016).

[21] J. Palacci, C. Cottin-Bizonne, C. Ybert, and L. Bocquet, Phys. Rev. Lett. **105**, 088304 (2010).

[22] I. Theurkauff, C. Cottin-Bizonne, J. Palacci, C. Ybert, and L. Bocquet, Phys. Rev. Lett. **108**, 268303 (2012).

[23] B. ten Hagen, S. van Teeffelen, and H. Löwen, J. Phys. Condens. Matter **23**, 194119 (2011).

[24] P. Romanczuk, M. Bär, W. Ebeling, B. Lindner, and L. Schimansky-Geier, Eur. Phys. J. Spec. Top. **202**, 1 (2012).

[25] M. E. Cates and J. Tailleur, Annu. Rev. Condens. Matter Phys. **6**, 219 (2015).

[26] G. Gonnella, D. Marenduzzo, A. Suma, and A. Tiribocchi, C.R. Phys. **16**, 316 (2015).

[27] Y. Fily and M. C. Marchetti, Phys. Rev. Lett. **108**, 235702 (2012).

[28] G. S. Redner, M. F. Hagan, and A. Baskaran, Phys. Rev. Lett. **110**, 055701 (2013).

[29] F. Peruani, A. Deutsch, and M. Bär, Phys. Rev. E **74**, 030904(R) (2006).

[30] I. S. Aranson and L. S. Tsimring, Phys. Rev. E **67**, 021305 (2003).

[31] F. Ginelli, F. Peruani, M. Bär, and H. Chaté, Phys. Rev. Lett. **104**, 184502 (2010).

[32] J. Deseigne, O. Dauchot, and H. Chaté, Phys. Rev. Lett. **105**, 098001 (2010).

[33] T. Vicsek, A. Czirók, E. Ben-Jacob, I. Cohen, and O. Shochet, Phys. Rev. Lett. **75**, 1226 (1995).

[34] T. Vicsek and A. Zafeiris, Phys. Rep. **517**, 71 (2012).

[35] J. Toner and Y. Tu, Phys. Rev. Lett. **75**, 4326 (1995).

[36] J. Toner, Phys. Rev. E **86**, 031918 (2012).

[37] B. Mahault, X.-c. Jiang, E. Bertin, Y.-q. Ma, A. Patelli, X.-q. Shi, and H. Chaté, Phys. Rev. Lett. **120**, 258002 (2018).

[38] G. Grégoire and H. Chaté, Phys. Rev. Lett. **92**, 025702 (2004).

[39] A. P. Solon, H. Chaté, and J. Tailleur, Phys. Rev. Lett. **114**, 068101 (2015).

[40] J.-B. Caussin, A. Solon, A. Peshkov, H. Chaté, T. Dauxois, J. Tailleur, V. Vitelli, and D. Bartolo, Phys. Rev. Lett. **112**, 148102 (2014).

[41] K.-D. N. T. Lam, M. Schindler, and O. Dauchot, New J. Phys. **17**, 113056 (2015).

[42] F. Giavazzi, M. Paoluzzi, M. Macchi, D. Bi, G. Scita, M. L. Manning, R. Cerbino, and M. C. Marchetti, Soft Matter **14**, 3471 (2018).

[43] E. Sese-Sansa, I. Pagonabarraga, and D. Levis, Europhys. Lett. **124**, 30004 (2018).

[44] J. Barré, R. Chétrite, M. Muratori, and F. Peruani, J. Stat. Phys. **158**, 589 (2015).

[45] M. N. van der Linden, L. C. Alexander, D. G. A. L. Aarts, and O. Dauchot, Phys. Rev. Lett. **123**, 098001 (2019).

[46] X.-q. Shi and H. Chaté, arXiv:1807.00294.
[47] D. Geyer, D. Martin, J. Tailleur, and D. Bartolo, Phys. Rev. X **9**, 031043 (2019).
[48] See the Supplemental Material at http://link.aps.org/supplemental/10.1103/PhysRevLett.124.078001 for details regarding correlation functions, velocity distributions and analytical derivations of the main equations.
[49] E. Fodor, C. Nardini, M. E. Cates, J. Tailleur, P. Visco, and F. van Wijland, Phys. Rev. Lett. **117**, 038103 (2016).
[50] L. Caprini, U. M. B. Marconi, and A. Vulpiani, J. Stat. Mech. (2018) 033203.
[51] L. Caprini, U. M. B. Marconi, and A. Puglisi, Sci. Rep. **9**, 1386 (2019).
[52] U. M. B. Marconi, N. Gnan, M. Paoluzzi, C. Maggi, and R. Di Leonardo, Sci. Rep. **6**, 23297 (2016).
[53] Y. Yang, V. Marceau, and G. Gompper, Phys. Rev. E **82**, 031904 (2010).
[54] M. Bär, R. Großmann, S. Heidenreich, and F. Peruani, Annu. Rev. Condens. Matter Phys. **11** (2019).
[55] A. Suma, G. Gonnella, D. Marenduzzo, and E. Orlandini, Europhys. Lett. **108**, 56004 (2014).
[56] L. F. Cugliandolo, P. Digregorio, G. Gonnella, and A. Suma, Phys. Rev. Lett. **119**, 268002 (2017).
[57] L. Caprini, U. Marini Bettolo Marconi, A. Puglisi, and A. Vulpiani, J. Chem. Phys. **150**, 024902 (2019).
[58] T. F. F. Farage, P. Krinninger, and J. M. Brader, Phys. Rev. E **91**, 042310 (2015).
[59] M. Rein and T. Speck, Eur. Phys. J. E **39**, 84 (2016).
[60] J. Tailleur and M. E. Cates, Phys. Rev. Lett. **100**, 218103 (2008).
[61] M. Cates and J. Tailleur, Europhys. Lett. **101**, 20010 (2013).
[62] T. Speck, Eur. Phys. J. Spec. Top. **225**, 2287 (2016).
[63] A. P. Solon, J. Stenhammar, M. E. Cates, Y. Kafri, and J. Tailleur, New J. Phys. **20**, 075001 (2018).
[64] J. Stenhammar, A. Tiribocchi, R. J. Allen, D. Marenduzzo, and M. E. Cates, Phys. Rev. Lett. **111**, 145702 (2013).
[65] T. Speck, J. Bialké, A. M. Menzel, and H. Löwen, Phys. Rev. Lett. **112**, 218304 (2014).
[66] A. P. Solon, Y. Fily, A. Baskaran, M. E. Cates, Y. Kafri, M. Kardar, and J. Tailleur, Nat. Phys. **11**, 673 (2015).
[67] A. P. Solon, J. Stenhammar, R. Wittkowski, M. Kardar, Y. Kafri, M. E. Cates, and J. Tailleur, Phys. Rev. Lett. **114**, 198301 (2015).
[68] J. Bialké, J. T. Siebert, H. Löwen, and T. Speck, Phys. Rev. Lett. **115**, 098301 (2015).
[69] A. Patch, D. M. Sussman, D. Yllanes, and M. C. Marchetti, Soft Matter **14**, 7435 (2018).
[70] S. Mandal, B. Liebchen, and H. Löwen, Phys. Rev. Lett. **123**, 228001 (2019).